Mid-infrared silicon-on-sapphire waveguide coupled photonic crystal microcavities

Yi Zou, Swapnajit Chakravarty, and Ray T. Chen

Articles you may be interested in

High-Q contacted ring microcavities with scatterer-avoiding "wiggler" Bloch wave supermode fields
Appl. Phys. Lett. **104**, 201102 (2014); 10.1063/1.4878337

Integrated high-quality factor silicon-on-sapphire ring resonators for the mid-infrared
Appl. Phys. Lett. **102**, 051108 (2013); 10.1063/1.4791558

Digital resonance tuning of high- Q/V m silicon photonic crystal nanocavities by atomic layer deposition
Appl. Phys. Lett. **91**, 161114 (2007); 10.1063/1.2800312

Surface encapsulation for low-loss silicon photonics
Appl. Phys. Lett. **91**, 131117 (2007); 10.1063/1.2793820

Transmission filtering of a waveguide coupled to a stub microresonator
Appl. Phys. Lett. **89**, 101113 (2006); 10.1063/1.2345251

Mid-infrared silicon-on-sapphire waveguide coupled photonic crystal microcavities

Yi Zou,[1,a)] Swapnajit Chakravarty,[2,a)] and Ray T. Chen[1,a)]

[1]*Microelectronics Research Center, Department of Electrical and Computer Engineering, University of Texas at Austin, 10100 Burnet Rd., Austin, Texas 78758, USA*
[2]*Omega Optics, Inc., 8500 Shoal Creek Blvd., Austin, Texas 78757, USA*

We experimentally demonstrate a photonic crystal (PC) microcavity side coupled to a W1.05 photonic crystal waveguide fabricated in silicon-on-sapphire working in mid-IR regime at 3.43 μm. Using a fixed wavelength laser source, propagation characteristics of PC waveguides without microcavity are characterized as a function of lattice constant to determine the light line position, stop gap, and guided mode transmission behavior. The resonance of an L21 PC microcavity coupled to the W1.05 PCW in the guided mode transmission region is then measured by thermal tuning of the cavity resonance across the source wavelength. Resonance quality factor ~3500 is measured from the temperature dependency curve. © 2015 AIP Publishing LLC.
[http://dx.doi.org/10.1063/1.4929601]

Since their conceptual inception through the theoretical studies of Yablonovitch[1] and John,[2] photonic crystals (PCs) have generated significant interest in the scientific community due to their ability to guide and trap light in length scales of the wavelength of light. Due to the difficulty in the controlled introduction of defects in three-dimensional PCs, much of the research over the last two decades has focused on two-dimensional (2D) planar PC structures wherein the PC provides lateral in-plane optical confinement while confinement out-of-plane is provided by total internal reflection. Novel applications using the unique slow light characteristics of PCs have been demonstrated in optical interconnects,[3] optical modulation,[4] and optical memory and switches.[5] PC devices have shown extremely high sensitivities in both chip integrated absorption sensing[6] and in chemical and biological sensing,[7] compared to other integrated photonic technologies.

Most demonstrations of chem-bio sensing with 2D PC microcavities and waveguides have been in the near-IR telecom wavelengths around 1550 nm. Recently, integrated mid-infrared photonics has gained considerable attention due to the immense potential for new applications in optical interconnects and sensing.[8] The opportunity of mid-IR photonics in biosensing can be debated due the large absorption cross-section of water, which is the necessary medium for any biological diagnostics. However, the larger absorption cross-section of most chemicals makes mid-IR photonics a very promising platform for chemical sensing via on-chip optical absorption spectroscopy.

Mid-IR integrated photonics at present is still somewhat in infancy. While there is some consensus regarding suitable materials at wavelengths beyond 2 μm,[8,9] a significant challenge is the ability for efficient characterization due to limited availability of appropriate optical sources. In particular, characterization of PC structures has relied on widely wavelength tunable sources.

The silicon on sapphire (SoS) material platform is ideal for mid-IR integrated photonics. Sapphire has a transparent window up to 5.5 μm. Additionally, sapphire cladding provides a high refractive index contrast with the core silicon.[8,9] PC structures of any given dimension can be fabricated in SoS without the possibility of bending and buckling in free-standing silicon membranes from SOI. A photonic crystal waveguide (PCW)[10] and a normally incident isolated free-standing PC microcavity[11] were previously demonstrated in the SOI platform with tunable optical sources. Characterization of mid-IR photonic components on-chip have otherwise been restricted to strip and slot waveguide based structures at fixed single wavelength.[12–15]

We recently demonstrated a method to overcome the limitation of mid-IR tunable sources for PC characterization by employing a lattice constant based tuning method, which allowed us to efficiently characterize the propagation characteristics of PC waveguides in SoS in the mid-IR.[16] We also demonstrated holey and slotted PCWs in SoS and showed their enhanced sensitivity to detection of chemical warfare agents versus SoS strip waveguides and slot waveguides, via mid-IR absorbance sensing at 3.43 μm.[17]

In this paper, we provide the experimental demonstration of PC microcavities in SoS in the mid-IR. In contrast to normally incident PC microcavities in free-standing silicon membranes from SOI,[11] this paper provides the experimental demonstration of in-plane PC waveguide coupled PC microcavities in SoS in mid-IR. A combination of lattice constant engineering and temperature tuning is employed to characterize the frequency drop characteristics of a linear PC microcavity coupled to a PCW, using a single wavelength source at 3.43 μm.

The PCW comprises a W1.05 PCW where the width of the PCW is $1.05 \times \sqrt{3} \times a$, where a is the PC lattice constant. The PC microcavity investigated is linear Ln-type that has been used extensively for biosensing in SOI in the near-IR.[18,19] n denotes the number of missing air holes in a row parallel to the PCW. Several PC microcavities such as L3, L13, and L21 were investigated. Near-IR characterization of

a)Authors to whom correspondence should be addressed. Electronic addresses: yzou@utexas.edu; swapnajit.chakravarty@omegaoptics.com; and raychen@ uts.cc.utexas.edu. Fax: +1-512-471-8575
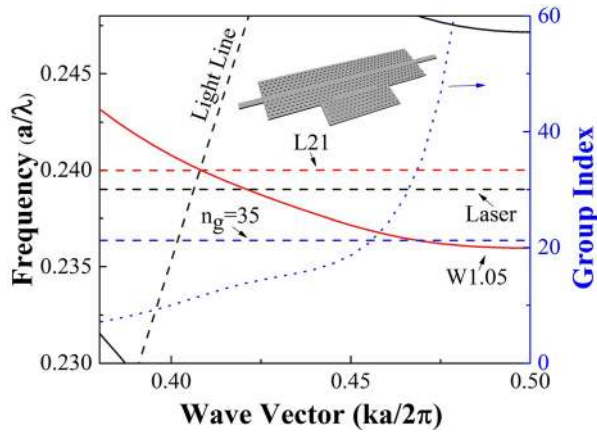
FIG. 1. Normalized dispersion diagram of W1.05 PCW in SoS with air top cladding. The W1.05 guided mode (red solid line) is shown together with frequency of resonant mode closest to the band edge for L21 PC microcavities by red dashed line. The black dashed line indicates the frequency of probe laser. The blue dotted line indicates the group index for guiding mode. The blue dashed line indicates the normalized frequency with $n_g = 35$. Sapphire light line is superimposed. The inset shows the schematic of L21 PC microcavity side coupled to W1.05 PCW device.

the above PCW coupled PC microcavities have shown a single drop resonance in L3 coupled PCW, and several dropped resonances in both L13 and L21 coupled PCWs.[18] For multi-resonance cavities, we have previously shown that the resonance closest to the W1 PCW transmission band edge has higher sensitivity than resonances further away from the band edge due to the enhanced slow light effect near the transmission band edge.[20] Fig. 1 shows the dispersion diagram of a W1.05 PCW via three-dimensional (3D) plane-wave expansion (PWE) simulation. The radius of the PC air holes is $r = 0.225a$, which gives a 40 nm PCW guided mode bandwidth compared to a 22 nm guided mode bandwidth previously.[16] The normalized resonance frequency of the resonance closest to the transmission band edge for a L21 PC microcavity is shown by red dashed lines in Fig. 1. For efficient in-plane coupling with high quality factor resonance, it is desired that the PC microcavity resonance couples to the W1.05 PCW below the sapphire light line. Due to its high refractive index ($n = 1.7$), the low-lying sapphire light imposes limitations on the possible PC microcavity geometries. When all lattice air holes have the same diameter, it was observed that only the L21 PC microcavity and PC microcavities longer than L21 have at least one resonance that

couples to the W1.05 PCW below the sapphire light line. We therefore selected the L21 PC microcavity for characterization. The blue dashed line shown in Fig. 1 shows the position on the dispersion diagram, where $n_g = 35$ in the fabricated device. Our experience in the near-IR shows that due to high propagation losses (that varies as $n_g{}^2$) at high group indices, the experimentally observed transmission band edge in PCW structures occurs roughly at the position on the dispersion diagram, where $n_g \sim 35$.[21]

W1.05 PCW devices without microcavities were first fabricated for different lattice constants, as previously described,[16] to determine the range of lattice constants for which the single wavelength Thorlabs interband cascade laser (ICL) at 3.43 μm propagates via the guided mode of the PCW. Sub-wavelength grating (SWG) couplers from previous research[15] were integrated with the PC microcavity devices, to couple light into and out of the SoS chips using single mode ZrF$_4$ mid-IR optical fibers. Light was coupled into the PC waveguides from input strip waveguides. A group index adiabatic taper is designed at both the input and output ends of the W1.05 PCW, as previously demonstrated, for efficient coupling of light between strip waveguides and PCWs with low Fresnel reflection losses at the interfaces.[21,22] The input fiber is not polarization sensitive. We make the assumption that the input light is equally split between the two orthogonal TE and TM polarizations. However, the grating couplers have polarization selectivity ratio of TE to TM as 18:1. Hence, the TE polarized light is preferentially coupled into the PCW. Details of the device fabrication and the experimental setup have been reported previously.[15]

Fig. 2 shows the transmitted light intensities at 3.43 μm through 80 μm long PCWs of different lattice constants. Zero propagation is observed for lattice constants smaller than $a = 810$ nm. Thus, for a smaller than 810 nm, our 3.43 μm wavelengths falls in the stop gap of the W1.05 PCW and hence does not propagate. Consistent with our previous observations in a low bandwidth PCW, in our current design, a bulge in the transmission intensity versus lattice constant profile is observed at lattice constants around $a = 820$ nm. To validate that the sapphire light line is around $a = 825$ nm, propagation loss measurements were done for several lattice constants $a = 815$ nm, 820 nm, 825 nm, and 830 nm, respectively. At lattice constants greater than $a = 825$ nm, the 3.43 μm source propagates though the PCW above the
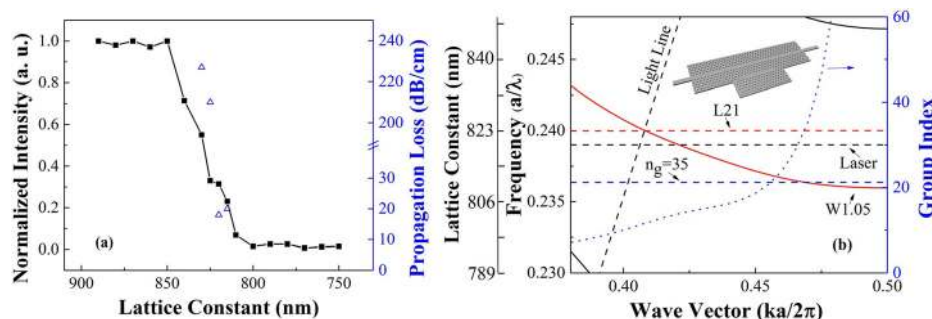

FIG. 2. (a) Normalized transmitted intensity through an 80 μm air-clad W1.05 PCW in SoS with $r = 0.25a$, as a function of a at $\lambda = 3.43$ μm (left axis), and propagation loss for several lattice constants to verify the guiding mode region (right axis). (b) Normalized dispersion diagram in Fig. 1. The vertical normalized frequency axis is multiplied by the fixed laser wavelength 3430 nm, and plotted, showing the approximate operating point of the fixed wavelength laser on the PCW dispersion diagram at different lattice constant.
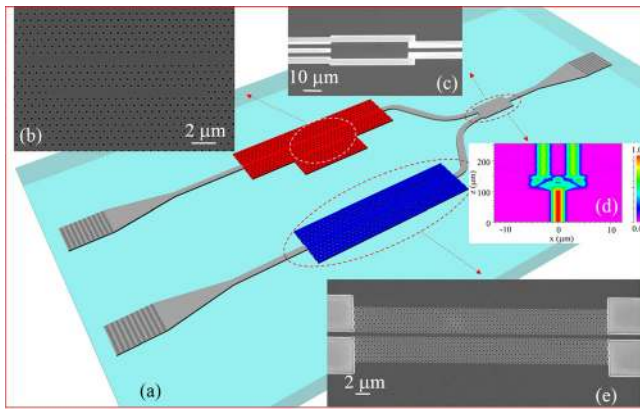
FIG. 3. (a) Schematic of the whole device. (b) L21 PC microcavity side coupled to W1.05 PCW. (c) 1×2 MMI for power splitting. (d) Simulated electrical field distribution for 1×2 MMI power splitter. (e) W1.05 PCW which serves as a reference channel.

sapphire light line and is thus extremely lossy. Therefore, although high propagation is observed for the short PCWs at a greater than 825 nm, for long PCWs, the propagation loss dominates and reaches as high as 227 dB/cm for $a = 830$ nm. Below the light line, for lattice constants $a = 815$ nm and $a = 820$ nm, respectively, the 3.43 μm light propagates via the W1.05 PCW guided mode with only 20 dB/cm loss and 18 dB/cm, respectively, comparable to previous demonstrations.[16] At $a = 820$ nm, our fixed wavelength laser light propagates just below the light line through the corresponding PCW. By comparing with the dispersion diagram, one notes that the fixed wavelength laser source propagates with higher n_g through $a = 815$ nm PCW than $a = 820$ nm. In Fig. 2(b), we plot the normalized dispersion diagram from Fig. 1 as a

function of lattice constant by multiplying the normalized frequencies with the fixed wavelength ($\lambda = 3.43 \mu$m) of our source laser. In the modified dispersion diagram shown in Fig. 2(b), the bandedge locates around $a = 810$ nm while intersection of guiding mode and the light line is around $a = 823$ nm. Both of them agree well with the experimental observations. The L21 PC microcavity resonances also couples to the W1.05 PCW just below the sapphire light line. $a = 820$ nm is therefore chosen to demonstrate the L21 PC microcavity coupled to the W1.05 PCW.

In order to demonstrate the drop characteristics of the L21 PC microcavity, the light from the input SWG is split into two paths via a 1×2 multimode interference (MMI) power splitter. The MMI is designed to be 11 μm wide and 51 μm long to split the light into two arms equally. An 80 μm long W1.05 PCW with $a = 820$ nm is fabricated in one arm. On the other arm, an 80 μm long W1.05 PCW coupled to a L21 PC microcavity is fabricated. The light from each channel is output to individual output SWGs. A schematic of the device is shown in Fig. 3(a). Figs. 3(b)–3(e) show scanning electron micrograph (SEM) images of the PCW, MMI, and PC microcavity coupled PCW devices.

The chip is mounted on a temperature controlled stage and the temperature scanned from 25 °C to 42 °C. Fig. 4(a) shows the normalized transmission through each arm of the MMI as a function of temperature. A drop in transmitted intensity is observed between 33 °C and 40 °C in the MMI arm with the PC microcavity. No significant change in transmitted intensity is observed for the MMI arm without the PC microcavity across the entire temperature range scanned. The power transmitted through the MMI arm with the PC microcavity is normalized versus the MMI arm without the
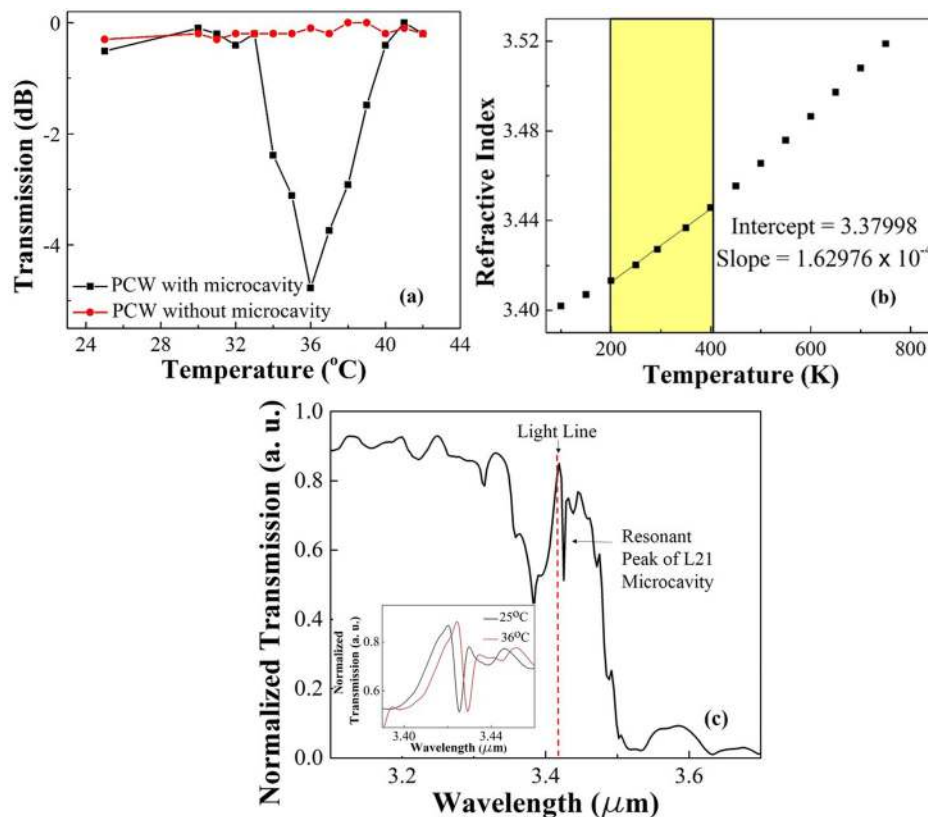

FIG. 4. (a) Normalized transmission variations versus temperature change for the two arms of our device. (b) Temperature dependency of refractive index of Si from Ref. 23. Slope and intercept values are calculated from linear fit inside yellow region. (c) 3D FDTD simulated transmission spectrum through an 80 μm long PCW with a side coupled L21 PC microcavity with $a = 820$ nm. The inset shows the resonance wavelength shift when temperature changes from 25 °C to 36 °C.

PC microcavity. The quality factor of the resonance is calculated from the temperature dependent transmission curve. The quality factor (Q) of a resonance is given by

$$Q = \frac{\lambda_0}{\Delta\lambda}.$$ (1)

Here, λ_0 and $\Delta\lambda$ are the center wavelength and the full width half maximum (FWHM) of the measured resonance respectively. $\Delta\lambda$ can be derived from the rate of change of λ with respect to temperature T, which can be solved by using chain rule as the following equation:

$$\Delta\lambda = \Delta T \frac{\partial\lambda}{\partial T} = \Delta T \frac{\partial\lambda}{\partial n}\frac{\partial n}{\partial T},$$ (2)

$\partial n/\partial T$ is the temperature dependency for refractive index, which is obtained from literature[23] while resonance wavelength shift due to refractive index change is obtained from FDTD simulation. We first calculate $\partial n/\partial T$ based on the data from Ref. 23. Good linearity is shown inside the yellow region in Fig. 4(b). $\partial n/\partial T \sim 1.62976 \times 10^{-4}$ RIU/K can be derived from the fit for the temperature range from 200 K to 400 K. The transmission spectrum for our side coupled L21 PC microcavity device with lattice equal 820 nm is simulated by 3D FDTD and plotted in Fig. 4(c). The position of the light line is shown by the dashed line. As shown in inset of Fig. 4(c), the resonance wavelength shifts about 3.58 nm when refractive index of Si changes around 1.79×10^{-3} RIU giving $\partial\lambda/\partial n \sim 1997$ nm/RIU. Thus, the calculated $\Delta\lambda$ from temperature dependent transmission curve is around 0.98 nm. From Eq. (1), we get $Q \sim 3500$ for the selected resonance of our side coupled L21 PC microcavity.

In summary, we demonstrate a side coupled PC microcavity in SOS in mid-IR region. The experimental propagation characteristics of PCW without microcavity by using lattice constant scanning method agree well with simulated data. Quality factor of PC microcavity is obtained through thermal tuning to move the resonance dip across fixed wavelength of our probe laser. $Q \sim 3500$ is experimental demonstrated for the selected resonance in a L21 PC microcavity. To demonstrate shorter L-type PC microcavities, such as L3, the resonance frequency must be pulled below the light line in the dispersion diagram. Various methods have been demonstrated in the literature to modify the resonance frequency, such as by tuning the bulk air hole radius, or by tuning the position and radius of the edge air holes of the PC microcavity in the $\Gamma - K$ direction and is the subject of further design.

[1]E. Yablonovitch, Phys. Rev. Lett. **58**(20), 2059 (1987).
[2]S. John, Phys. Rev. Lett. **58**(23), 2486 (1987).
[3]S. P. Anderson, A. R. Shroff, and P. M. Fauchet, Adv. Opt. Technol. **2008**, 293531 (2008).
[4]A. Hosseini, X. Xu, H. Subbaraman, C.-Y. Lin, S. Rahimi, and R. T. Chen, Opt. Express **20**(11), 12318 (2012).
[5]T. Tanabe, M. Notomi, S. Mitsugi, A. Shinya, and E. Kuramochi, Opt. Lett. **30**(19), 2575 (2005).
[6]W.-C. Lai, S. Chakravarty, Y. Zou, and R. T. Chen, Opt. Lett. **38**(19), 3799 (2013).
[7]Y. Zou, S. Chakravarty, W.-C. Lai, C.-Y. Lin, and R. T. Chen, Lab Chip **12**(13), 2309 (2012).
[8]R. Soref, Nature Photon. **4**(8), 495 (2010).
[9]R. A. Soref, S. J. Emelett, and W. R. Buchwald, J. Opt. A: Pure Appl. Opt. **8**(10), 840 (2006).
[10]C. Reimer, M. Nedeljkovic, D. J. M. Stothard, M. O. S. Esnault, C. Reardon, L. O'Faolain, M. Dunn, G. Z. Mashanovich, and T. F. Krauss, Opt. Express **20**(28), 29361 (2012).
[11]R. Shankar, I. Leijssen, I. Bulu, and M. Lončar, Opt. Express **19**(6), 5579 (2011).
[12]T. Baehr-Jones, A. Spott, R. Ilic, B. Penkov, W. Asher, and M. Hochberg, Opt. Express **18**(12), 12127 (2010).
[13]F. Li, S. D. Jackson, C. Grillet, E. Magi, D. Hudson, S. J. Madden, Y. Moghe, C. O'Brien, A. Read, and S. G. Duvall, Opt. Express **19**(16), 15212 (2011).
[14]Z. Cheng, X. Chen, C. Y. Wong, K. Xu, C. K. Y. Fung, Y. M. Chen, and H. K. Tsang, Photon. J. IEEE **4**(1), 104 (2012).
[15]Y. Zou, H. Subbaraman, S. Chakravarty, X. Xu, A. Hosseini, W.-C. Lai, P. Wray, and R. T. Chen, Opt. Lett. **39**(10), 3070 (2014).
[16]Y. Zou, S. Chakravarty, P. Wray, and R. T. Chen, Opt. Express **23**, 6965 (2015).
[17]Y. Zou, S. Chakravarty, P. Wray, and R. T. Chen, Sens. Actuators B: Chem. **221**, 1094–1103 (2015).
[18]W.-C. Lai, S. Chakravarty, Y. Zou, and R. T. Chen, Opt. Lett. **37**(7), 1208 (2012).
[19]Y. Zou, S. Chakravarty, D. N. Kwong, W.-C. Lai, X. Xu, X. Lin, A. Hosseini, and R. T. Chen, IEEE J. Sel. Top. Quantum Electron. **20**(4), 171 (2014).
[20]W.-C. Lai, S. Chakravarty, Y. Zou, Y. Guo, and R. T. Chen, Appl. Phys. Lett. **102**(4), 041111 (2013).
[21]Y. Zou, S. Chakravarty, L. Zhu, and R. T. Chen, Appl. Phys. Lett. **104**(14), 141103 (2014).
[22]S. Chakravarty, Y. Zou, W.-C. Lai, and R. T. Chen, Biosens. Bioelectron. **38**(1), 170 (2012).
[23]H. H. Li, J. Phys. Chem. Ref. Data **9**(3), 561 (1980).